IGS

Article

Corresponding author: Ken Kondo;
Email: kenkondo0410@gmail.com

Calving, ice flow, and thickness of outlet glaciers controlled by land-fast sea ice in Lützow-Holm Bay, East Antarctica

Ken Kondo[1,2] and Shin Sugiyama[1]

[1]Institute of Low Temperature Science, Hokkaido University, Sapporo, Japan and [2]Graduate School of Environmental Science, Hokkaido University, Sapporo, Japan

Abstract

To investigate the mechanisms driving recent changes in outlet glaciers in Antarctica, we measured the glacier front position, flow velocity and surface elevation of five outlet glaciers flowing into Lützow-Holm Bay in East Antarctica. After a steady advance from 2008 to 2015, all the glaciers synchronously retreated by 0.4–6.0 km between 2016 and 2018. The initiation of the retreat coincided with the breakup of land-fast sea ice in Lützow-Holm Bay in 2016, which resulted in the largest sea-ice loss in the region since 1998. Similar flow variations and surface elevation changes were observed near the grounding line of Shirase, Skallen and Telen glaciers. The slowdown in 2011–15 (by 13%) and the speedup in 2016–18 (by 7%) coincided with the respective increase and decrease in surface elevation. Simultaneous retreat and acceleration after the land-fast sea-ice breakup implies that sea ice has a significant influence on glacier dynamics. Thickening/thinning observed near the grounding line was attributed to a reduced/enhanced stretching flow regime during the deceleration/acceleration period. Our results demonstrate that land-fast sea ice affects not only terminus positions, but also the flow speed and ice thickness of the Antarctic glaciers.

1. Introduction

The Antarctic ice sheet has been losing mass for the past four decades, thereby contributing to a rise in sea level of 14 ± 2.0 mm during the period 1979–2017 (Rignot and others, 2019). The mass loss is caused by an increasing amount of ice discharge into the ocean, as observed in West Antarctica, the Antarctic Peninsula and Wilkes Land in East Antarctica (Pritchard and others, 2009; Smith and others, 2020a). In these regions, glacier flow has accelerated in association with changes in temperature and circulation of the ocean and the atmosphere (Gardner and others, 2018). The change in the flow regime of the glaciers has resulted in glacier thinning due to enhanced horizontal stretching of ice, a process known as dynamic thinning (Pritchard and others, 2009). Some of the large outlet glaciers in West Antarctica have shown a significant acceleration upstream of the grounding line, which is attributed to a loss of buttressing force from ice shelves. The ice shelves are thinning, and grounding lines are retreating under the influence of increased basal melting by the intrusion of warm and dense modified circumpolar deep water (mCDW) into the subshelf cavity (e.g. Shepherd and others, 2004; Dutrieux and others, 2014; Christianson and others, 2016). These processes have been studied on outlet glaciers flowing into the Amundsen Sea Embayment sector in West Antarctica, a dominant contributor to sea-level rise from the Antarctic ice sheet (Rignot and others, 2019; Shepherd and others, 2019). Grounding line retreat (Rignot and others, 2014), flow acceleration (Mouginot and others, 2014) and thinning (Pritchard and others, 2009; Smith and others, 2020a) have been observed in association with a strengthening of CDW inflow to the bay (Jacobs and others, 2011).

Other studies suggested that glacier dynamics are also influenced by changes in stress balance induced by iceberg calving from the glacier or ice-shelf front. In the Antarctic Peninsula, for example, rapid disintegration of Larsen A and B Ice Shelves triggered a significant speedup of the outlet glaciers feeding into the ice shelves (Rignot, 2004), resulting in increased ice discharge and mass loss (Wuite and others, 2015). To distinguish between these potential drivers of the Antarctic ice mass loss, detailed observations are needed on the ice speed, the front position and the ice thickness near the glacier front, since these factors control the discharge from the ice sheet (Dupont and Alley, 2005; Fürst and others, 2016).

In contrast to the rapid changes in West Antarctica and the Antarctic Peninsula, outlet glaciers in East Antarctica have been relatively stable according to observations over the past three decades (The IMBIE team, 2018). Previous studies in East Antarctica showed a link between glacier terminus variations and sea-ice concentrations (SIC) as well as air temperature (Miles and others, 2013, 2016; Baumhoer and others, 2021). Land-fast sea ice plays a role in terminus variations of glaciers in Antarctica, as it affects the stability of ice shelves by exerting buttressing force on the glacier front. A change in the buttressing effect has the potential to modify the glacier flow speed as well as the front position. For example, ice shelves in Porpoise Bay simultaneously disintegrated after the breakup of land-fast sea ice in front of the glaciers (Miles and others, 2017). Other studies of East Antarctica (Miles and others, 2013, 2016)

and Antarctica as a whole (Baumhoer and others, 2021) showed that long-term glacier advance and retreat coincided with positive and negative anomalies of SIC, respectively. Sea ice in front of glaciers also stabilize glacier termini by damping ocean swell reaching to the glacier fronts. In the Antarctic Peninsula, the disintegration of Larsen B Ice Shelf was deemed to be loss of sea ice because open water allowed storm-generated ocean swell to trigger extensive collapse of the ice shelf (Massom and others, 2018). An established link between sea ice and glacier change is important for the response of the Antarctic ice sheet to the rapidly changing climate, since land-fast sea ice is highly sensitive to climate change (Heil, 2006; Fraser and others, 2012; Aoki, 2017). However, studies focused on the impact of sea ice on East Antarctic glacier dynamics are scarce. Further studies are needed to improve understanding of ongoing glacier changes and their mechanisms in this region.

Lützow-Holm Bay, located in East Antarctica (69°S, 38°E), is usually covered by land-fast sea ice, which has shown quasiperiodic breakup events at intervals of 10–20 years (Ushio, 2006; Aoki, 2017). These breakups are deemed to be affected by atmospheric and oceanic conditions, including air temperature, southerly winds, sea surface temperature, SIC in the pack-ice zone and snowfall on the sea ice (Enomoto and others, 2002; Ushio, 2006; Aoki, 2017). The most recent breakup was observed in April 2016, when a large portion of the fast ice in the bay retreated (Fig. 1) (Aoki, 2017). Simultaneously, an iceberg conglomerate detached from Shirase Glacier, suggesting the influence of sea ice on the glacier terminus (Aoki, 2017). The breakup of land-fast sea ice possibly affected other outlet glaciers in Lützow-Holm Bay, but no investigations have been reported so far.

In this study, we carried out satellite observations of five outlet glaciers flowing into Lützow-Holm Bay to investigate recent glacier front variations with a focus on their relationship with sea-ice conditions. Glacier front positions, flow velocity and surface elevation in the period 1988–2020 were compared with SIC in front of the glaciers. Based on the results, we discuss possible influences of land-fast sea ice on the terminus position and dynamics of the studied glaciers.

2. Study site

This study focuses on five marine-terminating outlet glaciers flowing into Lützow-Holm Bay in East Antarctica: Shirase, Skallen, Telen, Honnør and Langhovde glaciers (69.20–70.17°S and 39.8–38.95°E) (Fig. 2). At the grounding line locations, the maximum ice speed ranges from 70 m a^{-1} (Langhovde Glacier) to 2200 m a^{-1} (Shirase Glacier), and the glacier width ranges from 2 km (Honnør Glacier) to 10 km (Shirase Glacier).

Shirase Glacier is the fastest flowing glacier in Lützow-Holm Bay. The ice shelf of Shirase Glacier disintegrates into large iceberg pieces, which aggregate and form a continuous floating ice tongue. The floating tongue significantly retreated six times in the period 1956–2016, and four of the events were associated with major breakups of land-fast sea ice in Lützow-Holm Bay (Pattyn and Derauw, 2002; Ushio, 2006; Nakamura and others, 2010; Aoki, 2017), suggesting the influence of sea-ice conditions on the glacier front position. Previous observations indicated that the breakup of land-fast sea ice also affected the ice flow of Shirase Glacier. Nakamura and others (2010) found a flow acceleration of the floating tongue in April–July 1998 that coincided with a major retreat of the land-fast sea ice in April 1998. After another sea-ice breakup in 2016, the glacier flow accelerated by 30% (Nakamura and others, 2022). The authors attributed the speedup to the loss of buttressing force exerted by the sea ice. These observations covered only the floating part of the glacier over periods less than three consecutive years (1996–98 and

2016–18). Thus, a possible link between sea ice and the grounded ice dynamics is not addressed. The glacier has shown a trend of mass gain for the last two decades, which was attributed to the reduction in the ice-shelf basal melting associated with a weakening of mCDW intrusion (Hirano and others, 2020; Kusahara and others, 2021; Miles and others, 2023). The grounding line of the glacier was reported to have advanced at a rate of 14.7 m a^{-1} between 2010 and 2016 (Konrad and others, 2018).

Airborne and in situ observations were conducted at Shirase and Langhovde glaciers by the Japanese Antarctic Research Expedition. The bedrock elevation of Shirase Glacier was measured by airborne radar-echo soundings in the 1980s (Wada and Mae, 1981; Mae and Yoshida, 1987). The survey results showed that the ice thickness was 880 m near the grounding line, above which the bed elevation was below sea level for 30 km. At ~200 km from the grounding line, rapid thinning (0.5–1.0 m a^{-1}) was observed by triangulation chain surveys conducted in the period 1969–74 (Naruse, 1979). The thinning was attributed to stretching ice flow enhanced by acceleration due to increased basal sliding (Mae and Naruse, 1978). This observation demonstrated the importance of glacier dynamics on the mass budget of the ice sheet, since ice-flow changes of the outlet glaciers have a significant impact on the thickness of inland ice (e.g. Nick and others, 2009).

Langhovde Glacier is located 20 km south of the Japanese research base, Syowa Station (Fig. 1a). In situ ice speed measurement on its several-kilometer-long ice shelf confirmed short-term velocity variations due to ocean tides (Sugiyama and others, 2014; Minowa and others, 2019). The glacier retreated by ~200 m in the summer of 2011 during a breakup event of land-fast sea ice in Lützow-Holm Bay, while no significant change was observed in the surface elevation from 2006 to 2012 (Fukuda and others, 2014).

Glaciological studies of Honnør, Skallen and Telen glaciers are scarce. The ice flow speeds of Skallen and Telen glaciers were measured during the period 2007–11 using satellite data (Shiramizu, 2018). Interannual velocity variations were reported, but the mechanisms of the changes remained unclear.

3. Data and methods

3.1. Terminus position

The frontal margins of the studied glaciers were mapped during the period 1988–2020, using satellite images obtained by the Japanese Earth Resources Satellite-1 (JERS-1) synthetic aperture radar (SAR), Advanced Spaceborne Thermal Emission and Reflection (ASTER) radiometer, Landsat 4 Thematic Mapper (TM), Landsat 7 Enhanced Thematic Mapper Plus (ETM+) and Landsat 8 Operational Land Imager (OLI). Relatively large geolocation errors due to inaccurate co-registration found in the JERS-1 SAR and Landsat 4 TM images were corrected against the Landsat 8 OLI image acquired on 11 March 2020, by adjusting the coordinates of commonly observed bedrock features with the horizontal shift of 0.3–0.7 km.

We utilized backscatter images from JERS-1 SAR, the visible and near-infrared band 3N from ASTER, true-color composites from Landsat 4 TM (bands 1–3), Landsat 7 ETM+ (bands 1–3) and Landsat 8 OLI (bands 2–4). In each image, the glacier fronts were manually delineated using geographic information software QGIS or Google Earth Engine Digitization Tool (Lea, 2018). The mapping was performed 40–65 times for each glacier, by analyzing 125 images in total. To obtain mean frontal displacement, a change in the ice surface area near the front was divided by the glacier width. To take into account the influence of curved flowline, we employed the curvilinear box method proposed by Lea
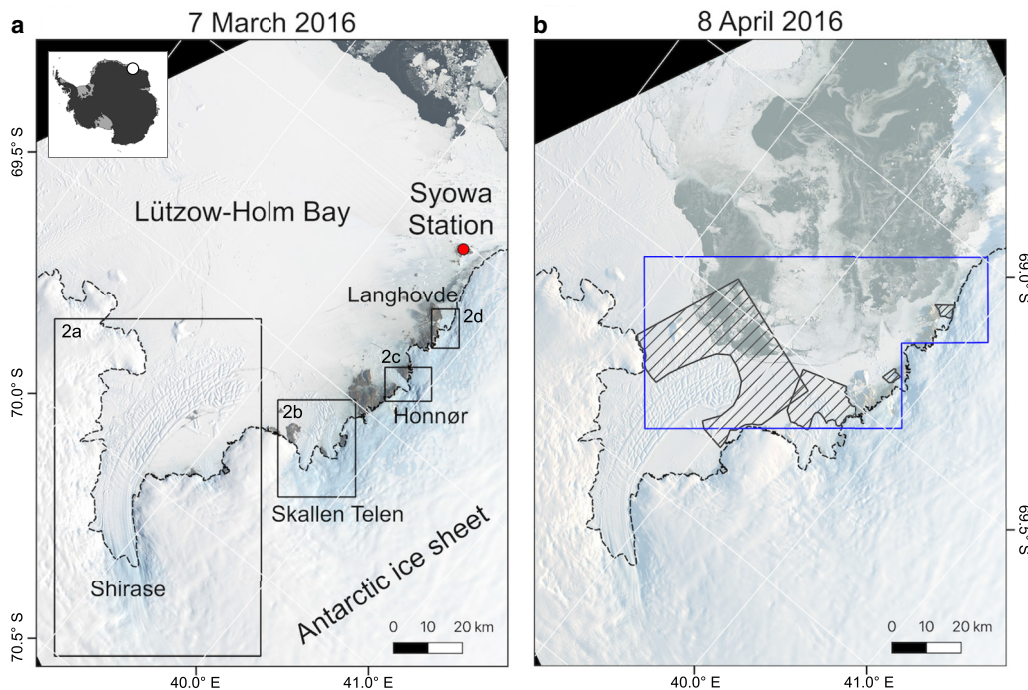
Figure 1. Landsat 8 OLI images of Lützow-Holm Bay acquired on (a) 7 March 2016 and (b) 8 April 2016, showing the studied area before and after the breakup of land-fast sea ice. The inset in (a) shows the location of the study site in Antarctica. The boxes in (a) indicate the studied glaciers and areas shown in Figure 2. The hatched polygons in (b) show the regions of interest (ROIs) in front of the glaciers, where sea-ice conditions were analyzed using satellite images. Sea-ice concentration data from Climate Data Record of Passive Microwave Sea Ice Concentration, Version 4 (Meier and others, 2021) were analyzed in the region indicated by the blue polygon in (b). The dashed line indicates the grounding line estimated by Fukuda (2014) for Langhovde Glacier and Bindschadler and others (2011) for the other regions.

and others (2014). Because it was difficult to distinguish the calving front of Shirase Glacier from the icebergs aggregated near the front, we measured the length of the floating ice tongue following Ushio and others (2006) and Aoki (2017). The distance from the grounding line to the forefront of the iceberg aggregate was measured along a flowline as shown by the example in Figure 2a.

Temporal resolution of the measurement was dependent on data availability. After a 5-year gap from 1989 to 1994, the resolution was ~1 year from 1994 to 2003 and finer from 2003 to 2020. To precisely measure the timing and magnitude of glacier retreat, all available images were used for mapping during the periods of retreat. The uncertainty in the measurement was estimated by mapping an ice-free coastline using 3–18 images for each sensor. The standard deviations of the coordinates along the coastline was 27 m for JERS-1, 21 m for ASTER, 21 m for Landsat 4, 24 m for Landsat 7 and 7 m for Landsat 8.

3.2. Ice flow velocity

The annual flow velocity of Shirase, Skallen and Telen glaciers was obtained for the period 2001–18 from the ITS_LIVE dataset (Gardner and others, 2019). The dataset provides velocity fields with a spatial resolution of 240 m, derived by applying a feature tracking algorithm auto-RIFT (Gardner and others, 2018) to the Landsat 4, 5, 7 and 8 imagery. Mean annual speeds near the grounding lines were obtained as a mean over the boxes shown in Figure 2. Speed profiles along the central flowlines shown in Figures 2a and b were also analyzed.

To study the details of the variations in velocity, we applied a feature tracking algorithm (Sakakibara and Sugiyama, 2014) to 125 image pairs of Landsat 7 ETM+ and Landsat 8 OLI imagery acquired over the period 2006–20. The objective of this measurement was (1) to obtain annual velocity fields of the smaller Langhovde and Honnør glaciers, which could not be resolved by the ITS_LIVE dataset and (2) to improve the spatial and

temporal resolutions of the velocity of Shirase, Skallen and Telen glaciers. The temporal separations of the image pairs ranged from 16 to 416 days. We used an automatic image matching scheme known as the orientation correlation method in a frequency domain (Heid and Kääb, 2012; Sakakibara and Sugiyama, 2020). Horizontal biases on the image pairs were removed by minimizing displacement vectors obtained in off-ice areas. We excluded vectors obtained with a low signal-to-noise ratio (<30) and those that deviated by more than 30° or 100 m a^{-1} from a median vector within 3×3 neighboring pixels (Heid and Kääb, 2012; Sakakibara and Sugiyama, 2014). Errors in velocity measurement are associated with (1) ambiguities in the cross-correlation peak, (2) co-registration errors and (3) false correlations (Howat and others, 2010). We evaluated (1) and (2) from the root-mean-square errors of horizontal displacement in off-ice areas where displacement was assumed to be zero. During the calculation of the root-mean-square errors, displacement greater than twice the pixel size was attributed to a false correlation and therefore excluded. Errors caused by (3) were minimized by applying a 3×3 median low-pass filter. Error estimates ranged between ±1 and ±115 m a^{-1} with a mean value of ±31 m a^{-1}. The error was dependent on the temporal separation of the image pairs, i.e. uncertainty was greater for shorter temporal separation. The magnitude of the velocity obtained near the grounding line of Langhovde Glacier was consistent with that of the ITS_LIVE dataset (within ±5%). Ice speed was averaged in space and time within the boxes near the grounding lines shown in Figure 2 to obtain mean annual speeds during the periods 2014–20 for Langhovde Glacier and 2006–20 for Honnør Glacier. We also utilized satellite-derived flow speeds reported by Fukuda and others (2014) for the region near the grounding line of Langhovde Glacier from 2003 to 2012.

Ice discharge from Shirase Glacier across a flux gate near the grounding line (Fig. 2a) was calculated for the years 2013 and 2015. Ice speed from the ITS_LIVE dataset was used with the
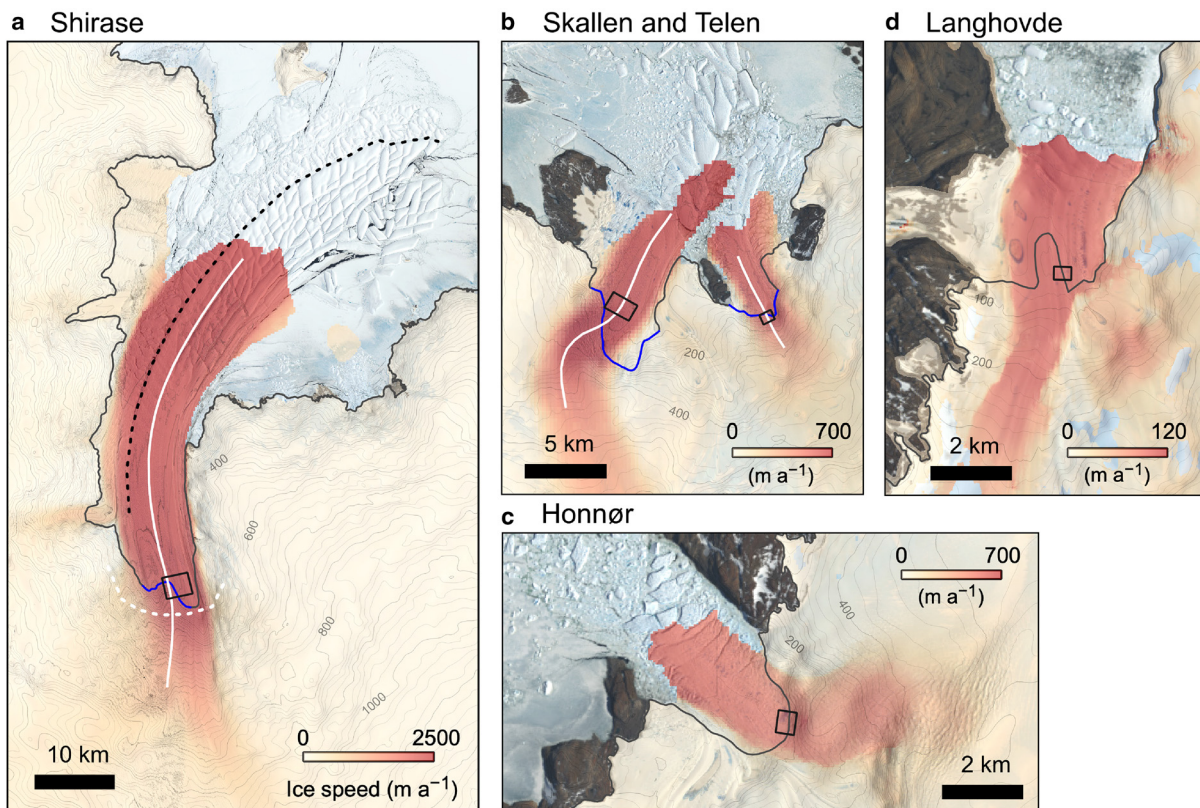
Figure 2. Landsat 8 OLI images acquired on 3 January 2016 showing the five studied glaciers flowing into Lützow-Holm Bay. The color scale shows the mean ice speed from 2001 to 2020. The solid black lines indicate the grounding line estimated by (a–c) Bindschadler and others (2011) and (d) Fukuda (2014). The blue lines in (a) and (b) indicate the grounding line estimated in this study, based on the change in surface slope observed with the Reference Elevation Model of Antarctica Strip digital elevation models acquired in 2013 and 2012, respectively. The boxes near the grounding line indicate areas used for the calculation of the ice speed shown in Figure 4. The dotted black line in (a) shows an example of a flowline used for the length measurement of Shirase Glacier. The solid white lines in (a) and (b) indicate the central flowlines used to plot the ice speeds shown in Figure 11. The dotted white line in (a) shows the flux gate used for the calculation of ice mass discharge from Shirase Glacier.

assumption of a full slip condition. Ice thickness was computed using surface elevation from digital elevation models (DEMs) on 6 January 2013 and 15 March 2016 (see section 3.3 for details) and bed elevation from BedMachine Antarctica, Version 3 (Morlighem and others, 2020; Morlighem, 2022). An ice density of 910 kg m^{-3} was assumed to convert the volume to mass flux. The uncertainty in the discharge was estimated at 10% according to the errors expected in the ITS_LIVE (<1%) and BedMachine datasets (10%).

Changes in flow regime affect vertical strain rate. To investigate this effect, the logarithmic strain rate (Nye, 1959) was calculated for Shirase, Skallen and Telen glaciers, using the annual glacier velocity field from the ITS_LIVE dataset. The calculation was performed at each velocity pixel, by employing the method and code provided by Alley and others (2018).

3.3 Glacier surface elevation

Changes in the surface elevation on Shirase, Skallen and Telen glaciers were measured with DEMs from the Reference Elevation Model of Antarctica (REMA) (Howat and others, 2019) using all available DEMs during 2012–16. We compared DEMs representing the austral summers 2012/13 and 2015/16, which were generated by averaging DEMs available from October 2012 to March 2013 and October 2015 to March 2016, respectively (Table 1).

To homogenize the REMA Strips distributed with a grid spacing of 2 or 8 m, those with a 2 m grid were resampled to 8 m by taking the average of the neighboring pixels. Horizontal and vertical shift, and elevation dependent biases were minimized by the co-registration and bias correction procedures introduced by Nuth and Kääb (2011) and Levinsen and others (2013). For this procedure, we used the REMA Mosaic DEM in off-ice areas and CryoSat-2 altimetry data over the ice sheet. The REMA Mosaic DEM was used as the elevation reference after excluding pixels from steep terrain (>30°). The CryoSat-2 altimetry data obtained at the point of closest approach are distributed by the European Space Agency CryoTEMPO project (Gourmelen and others, 2018). We utilized the altimetry data obtained within ±100 days from the DEM acquisition dates. All the elevation data were referenced to WGS-84 ellipsoid. The co-registration was performed in the region below 800 m. The standard deviations of the elevation of the REMA Strip DEMs against the REMA Mosaic DEM and CryoSat-2 altimetry data was between 0.3 and 2.4 m (Table 1).

We also utilized the GLAS/ICESat-1 and ICESat-2 data to measure the glacier surface elevation in 2003/04 and 2019/20, respectively. The GLA06 version 34 product of ICESat-1

Table 1. The REMA Strip DEMs used in this study

Region	Period	Acquisition date	σ_e (m)
Shirase	2012/13	25 December 2012	0.9
		6 January 2013	2.4
	2015/16	15 March 2016	1.4
Skallen/Telen	2012/13	7 December 2012	0.3
	2015/16	12 October 2015	0.9
		16 October 2015	0.8

The standard deviations of the DEMs from the reference (the REMA Mosaic DEM and CryoSat-2) are shown (σ_e)

(Zwally and others, 2014) obtained between October 2003 and October 2004 and the ATL06 Land Ice Height version 3 product of ICESat-2 (Smith and others, 2020b) obtained between May 2019 and June 2020 were downloaded from OpenAltimetry (Khalsa and others, 2020). The accuracy of the altimetry was 0.15 m for ICESat-1 (Shuman and others, 2006) and 0.03 m for ICESat-2 (Brunt and others, 2019).

The DEMs were analyzed with QGIS to estimate the grounding line positions from the inflection points of the surface slope (Fricker and Padman, 2006). The mean displacement of the grounding line between 2012/13 and 2015/16 was calculated by the box method as described in section 3.1.

3.4. Sea ice

Open water and ice-covered ocean areas were measured from 2000 to 2020 in the regions of interest (ROIs) defined near the glacier fronts as shown in Fig. 1b. The same ROI was given to Skallen and Telen glaciers, due to their proximity. The ASTER L1T Radiance and Landsat 7/8 Collection 1 top of atmosphere (TOA) reflectance products with a spatial resolution of 30 m were analyzed in Google Earth Engine for this purpose. The ASTER L1T Radiance was converted to TOA reflectance using coefficients provided by the distributers. We analyzed between 538 and 778 images for each glacier to classify pixels within the ROIs as being open water, ice or cloud. Thresholds for the classification were determined for each satellite, based on a manually classified dataset. The manual classification was performed for 27 images for ASTER (10.0×10^6 pixels), 17 for Landsat 7 (19.7×10^6 pixels) and 17 for Landsat 8 (20.5×10^6 pixels), which covered a wide range of illumination conditions and seasons.

Before the ocean surface classification took place, cloud pixels were eliminated based on the TOA reflectance at the shortwave infrared (SWIR) band and the normalized difference snow index (NDSI). Cloud pixels were selected for their high reflectance in the SWIR band (Moussavi and others, 2020), whereas NDSI was able to distinguish clouds from snow surface (Hall and others, 1995; Moussavi and others, 2020). Pixels were regarded as cloud when the TOA SWIR reflectance and NDSI were >0.1 and <0.65 for ASTER and >0.06 and <0.8 for Landsat 7/8, respectively. This procedure eliminated 98% of the pixels manually classified as cloud. After removing scenes with >20% cloud cover over the ROIs, the remaining pixels were classified either as open water or as ice, based on TOA reflectance at the green band for ASTER and the panchromatic band for Landsat 7/8. For all the sensors, pixels with a reflectance ≥0.25 were classified as ice (sea ice, iceberg or ice mélange), whereas those with <0.25 were classified as open water. The results obtained by this procedure concurred with manual classification in the case of 99% of the pixels.

Sea-ice conditions in Lützow-Holm Bay were analyzed by the Climate Data Record of Passive Microwave Sea Ice Concentration, Version 4 (Meier and others, 2021) provided by the National Oceanic and Atmospheric Administration's (NOAA) National Snow and Ice Data Center (NSIDC). We averaged monthly SIC data obtained at seven data cells, which covered the area indicated by the blue line in Figure 1b. Monthly anomalies were calculated using the mean from 1988 to 2020 as a reference.

3.5. Meteorological data

The mean summer air temperature (for December, January and February) was calculated for the period 1988–2020, using hourly data measured at Syowa Station (69.00°S, 39.58°E, 29 m a.s.l.) and distributed by the Japan Meteorological Agency. The station is located on the coast of Lützow-Holm Bay, 20–110 km north of the studied glaciers (Fig. 1a).
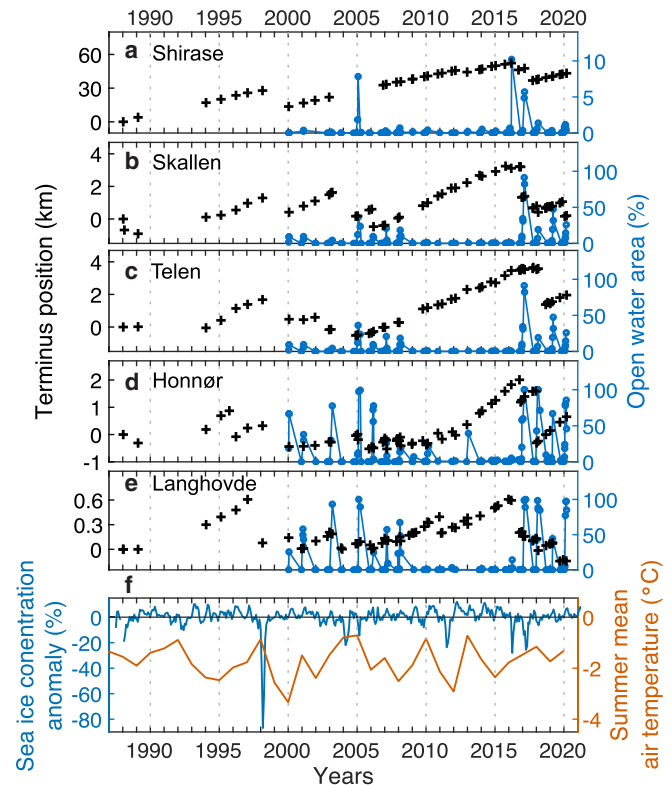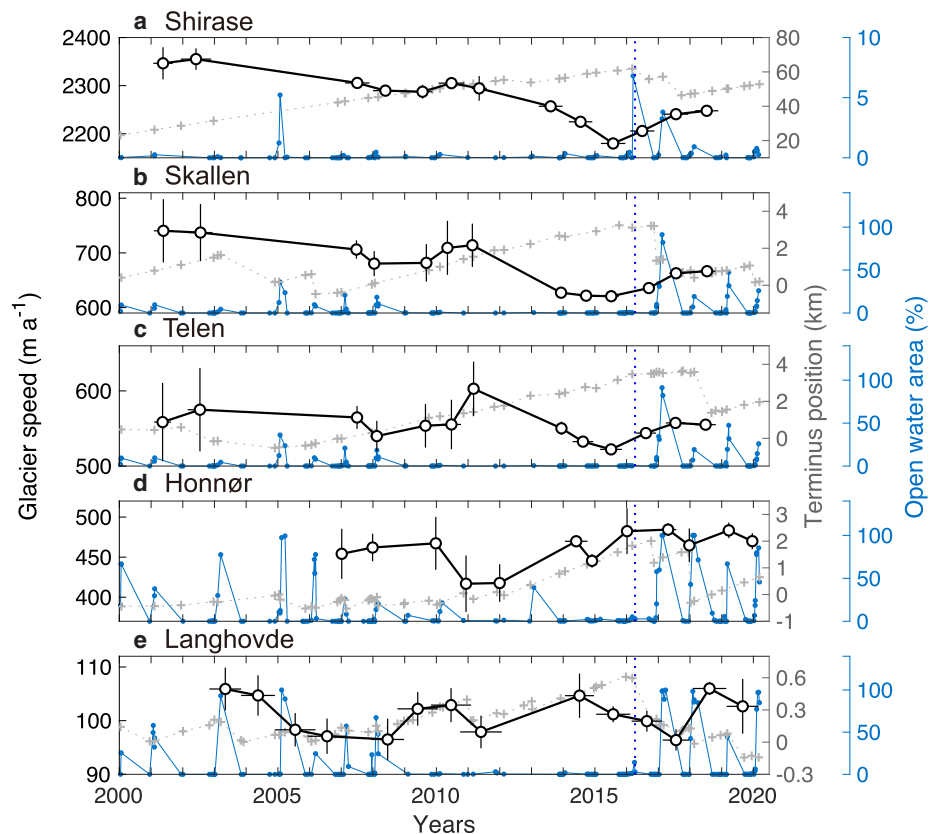

Figure 3. Terminus position relative to 1988 (crosses) and fraction of open water area within the ROIs shown in Figure 1b (circles) for (a) Shirase, (b) Skallen, (c) Telen, (d) Honnør and (e) Langhovde glaciers. (f) Monthly sea-ice concentration anomaly in Lützow-Holm Bay (blue), mean summer (December, January and February) air temperature at Syowa Station (orange).

4. Results

4.1. Terminus position and sea-ice conditions

The studied glaciers showed similar frontal variations, characterized by a steady advance and interrupted by at least three retreat events (Figs 3a–e). From 1994 to 1997, the studied glaciers advanced steadily without noticeable retreat, with the exception of Honnør Glacier, which retreated by 0.9 km in 1995–96. During 1997–98, Langhovde Glacier retreated by 0.5 km, and the other glaciers retreated in the period 1998–2000, resulting in the removal of 130 km² of glacier ice in total. After the retreat between 1997 and 2000, all the glaciers advanced from 2000 to 2016. Shirase Glacier advanced until 2012, at which time it was interrupted by the disintegration of a 1.5 km-long floating tongue in the period December 2012–November 2013 (Fig. 3a). Skallen Glacier steadily advanced until 2016, except for a retreat of 2.1 km in the period February 2003–March 2006 (Fig. 3b). The other three glaciers were relatively stable between 2000 and 2008, followed by an advance from 2008 to 2016 without significant loss of ice due to calving (Figs 3c–e). In 2016–18, all the studied glaciers retreated simultaneously at the greatest rate recorded during the observation period. Between March and October 2016, Shirase and Langhovde glaciers retreated by 6.0 and 0.4 km, respectively (Figs 3a, e). Skallen and Honnør glaciers retreated between October and December 2016 by 1.8 and 0.8 km, respectively (Figs 3b, d). These four glaciers continued to retreat until the summer of 2018. Telen Glacier retreated by 2.2 km slightly later – between February and September 2018 (Fig. 3c). In total, 200 km² of ice was lost in the studied glaciers over the period 2016–18. In 2019–20, Skallen and Langhovde glaciers further retreated by 0.9 and 0.3 km, respectively (Figs 3b, e).

The observed glacier front variations were associated with variations in SIC (Figs 3a–e). In general, the open water area dropped

Figure 4. Mean annual glacier speeds (open circles) at the grounding line (averaged in the polygons in Fig. 2), terminus positions relative to 1988 (crosses) and the fraction of open water areas within the ROIs shown in Figure 1b (closed circles) at (a) Shirase, (b) Skallen, (c) Telen, (d) Honnør and (e) Langhovde glaciers. The length of the horizontal and vertical lines associated with the markers show the mean time separation of image pairs used for velocity calculations and uncertainty in glacier speed, respectively. The vertical dotted line indicates the timing of the land-fast sea-ice breakup in April 2016.

below 10% between September and November and peaked between January and March. During the summer months of 2000–08, when the glacier front positions were relatively stable, the fraction of the open water area increased to >20% near the front of Honnør and Langhovde glaciers (Figs 3d, e). From January to February 2005, open water in front of Shirase, Skallen/Telen, Honnør and Langhovde glaciers increased to 8, 36, 99 and 99%, respectively. Sea ice in Lützow-Holm Bay recovered after 2008. From 2009 to 2015, the observation of open water areas was consistently lower than 5%, except for an increase at Honnør Glacier in the summer 2010 (21%) and 2013 (40%). The period of stable sea ice corresponded with a simultaneous advance of the glacier fronts (Figs 3a–e). The most significant sea-ice loss during the period of this analysis was the breakup of land-fast ice in April 2016 (Fig. 3f). The greatest extent of open water over the studied period was recorded in March 2016 at Shirase Glacier (10%) and February 2017 at the other glaciers (91% at Skallen/Telen, 100% at Honnør and Langhovde). The period of sea-ice loss coincided with the onset of rapid glacier retreat since 2016. Near Shirase Glacier, the open water area increased to 6% the following summer (2016/17), followed by more stable sea-ice conditions (<2% open water) from 2018 to 2020 (Fig. 3a). Near the ice front of Honnør and Langhovde glaciers, open water expanded to >85% in the summer of 2017, 2018 and 2020, indicating that the impact of the breakup of land-fast sea ice in 2016 has persisted over the following 4 years (Figs 3d, e).
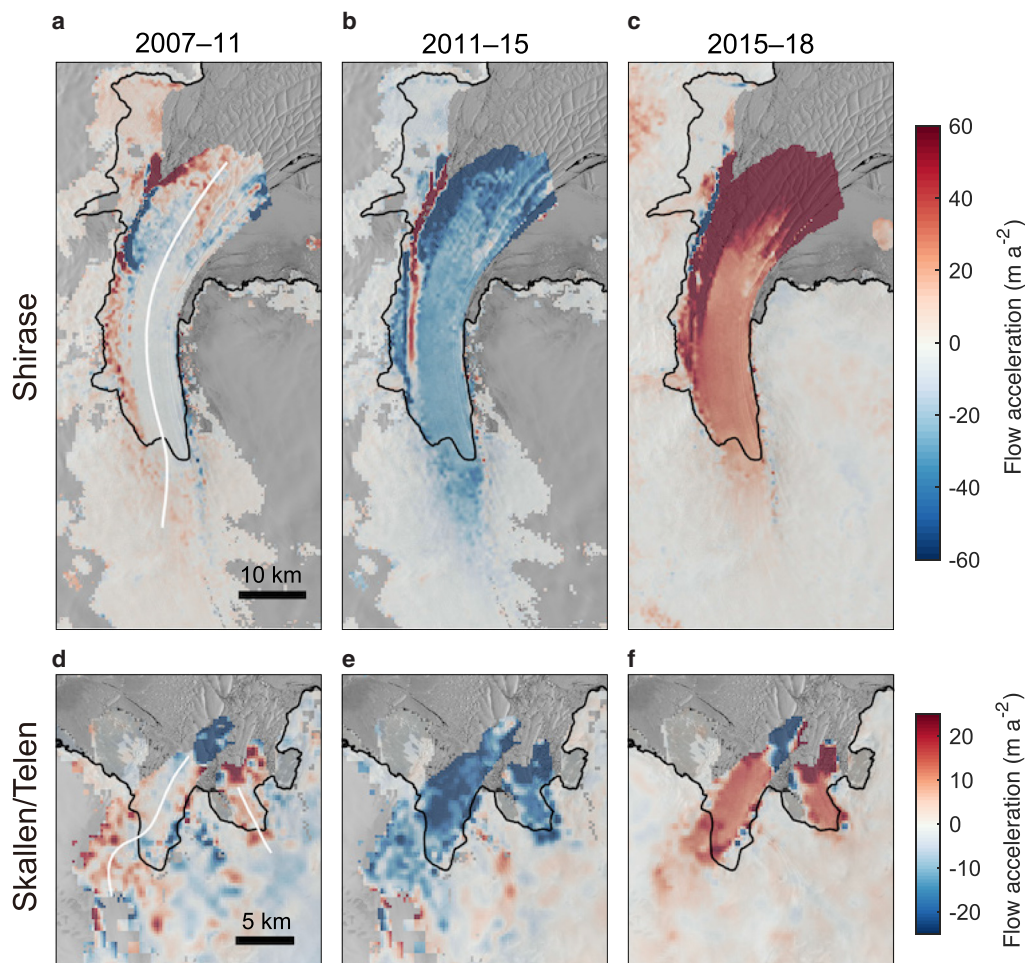
4.2. Glacier speed

The annual ice speed of each glacier varied within 7–18% of its mean over the period of the study. Shirase, Skallen and Telen glaciers showed similar flow variations in terms of timing and magnitude, with a slowdown from 2011 to 2015 and a speedup after 2016 (Figs 4a–c), whereas smaller, more frequent variations were observed at Honnør and Langhovde glaciers (Figs 4d, e).

The ice speed at Shirase Glacier decreased from 2002 to 2015 by 180 m a^{-1} (Fig. 4a), with the most substantial slowdown of 80 m a^{-1} from 2013 to 2015. Skallen and Telen glaciers decelerated in 2011–15 (−90 and −80 m a^{-1}) after a short period of acceleration in 2009–10. At Shirase, Skallen and Telen glaciers, the slowest speeds over the study period were observed in 2015 (2180, 620 and 520 m a^{-1}, respectively). By 2018, the flow of these three glaciers had accelerated to 2250, 670 and 560 m a^{-1}, respectively.

Honnør Glacier decelerated from 2009 to 2010, after a relatively stable speed during 2007–09 (Fig. 4d). The speed increased from 420 to 470 m a^{-1} from 2012 to 2014. Thereafter, the glacier speed was stable within 450–480 m a^{-1} until 2020. The speed of Langhovde Glacier showed fluctuations with relatively fast flow (>100 m a^{-1}) in the years 2003–04, 2009–10, 2014–15 and 2018–19 (Fig. 4e).

Spatial patterns of flow acceleration on Shirase, Skallen and Telen glaciers show further details of the synchronous ice speed changes observed at these three glaciers (Fig. 5). From 2007 to 2011, only small changes were observed in limited areas near the glacier fronts (Figs 5a, d). During this period, the rates of mean speed changes along the central flowline of each glacier (white lines in Figs 5a, d) were within ±5 m a^{-2}. Substantial changes were observed in 2011–15 and 2015–18 in the areas downstream of the grounding lines. Shirase Glacier decelerated in 2011–15, with the most pronounced changes (−60 m a^{-2}) observed near the glacier front (Fig. 5b). Thereafter, the terminus area accelerated in the period 2015–18 at a rate of 80 m a^{-2} (Fig. 5c). These speed changes extended upstream of the grounding lines. For example, the speed 10 km upstream of the grounding line decreased by 28 m a^{-2} in 2011–15 and increased by 23 m a^{-2} in the period 2015–18. Similarly, Skallen and Telen glaciers showed the greatest speed changes downstream of the grounding lines, and large variations were also observed upstream of the grounding line (Figs 5e, f). Along the central flowlines, a deceleration in the years 2011–15 (−17 and −15 m a^{-2} for Skallen and Telen,

Figure 5. Ice speed acceleration from the ITS_LIVE dataset at (a–c) Shirase and (d–f) Skallen/Telen glaciers during the periods (a and d) 2007–11, (b and e) 2011–15 and (c and f) 2015–18. The background is a Landsat 8 OLI image acquired on 3 January 2016. White lines (a and d) show central flowlines used to measure the ice speed changes described in the text.

respectively) was followed by an acceleration in the period 2015–18 (11 m a^{-2} for both glaciers).

To better understand glacier acceleration observed after 2015, we analyzed the displacement of sea ice near the fronts of Shirase, Skallen and Telen glaciers, by applying the feature tracking algorithm to the Landsat 8 OLI images acquired from October 2014 to February 2016 (Fig. 6). Sea-ice displacement prior to the breakup in 2016 was substantially less than the forward motion of the glacier terminus. For example, the displacement of the sea ice 10 km off Shirase Glacier was 50% of the glacier front motion (Fig. 6b). From January to February 2016, the displacement rate of the sea ice increased by 1000 m a^{-1}, reaching ∼90% of the glacier speed (Fig. 6c). A similar speedup was observed on the sea ice near the front of Skallen Glacier, showing a twofold increase from the summer 2014/15 to 2015/16 (Figs 6e, f).

4.3. Glacier surface elevation

Near the grounding line of Shirase Glacier, surface elevation increased from 2003 to 2012/13 (Figs 7a, 8a). The mean elevation change along a track of ICESat-1 located 0–5 km downstream of the grounding line (AA' in Fig. 7b) was 5.9 ± 0.3 m. The elevation increase was more rapid in the following period (2012/13–16). The magnitude of the mean changes was 3.1 ± 0.3 m along AA' and 5.5 ± 0.1 m along the ICESat-2 track BB' located 0–6.5 km downstream of the grounding line (Figs 7b, 8). An even greater increase of 6.5 ± 0.2 m was observed as a mean along the ICESat-2 track CC' crossing the grounding line. The greatest

elevation change along the track AA' from 2003 to 2016 was 27 ± 1 m (2.2 ± 0.1 m a^{-1}) at 3.5 km from the western margin (Fig. 8a). In the following period (2016–20), the elevation increase continued at a reduced rate along BB' (mean of 1.60 ± 0.06 m) (Figs 7c, 8b), whereas the surface dropped along CC' (mean of −0.8 ± 0.1 m) (Fig. 7c). A large amount of positive and negative elevation changes were observed 15 km downstream of the grounding line. These changes were attributed to the advection of surface topographic features (e.g. bumps and depressions).

A substantial change in surface elevation was also observed on Skallen Glacier. Along the ICESat-1 track crossing the grounding line (DD' in Fig. 7e), the mean surface elevation change from 2004 to 2012 was 0.87 ± 0.06 m (Fig. 7d). Greater changes were observed in the period 2012–15, reaching 2.4 ± 0.2 m as a mean along DD' (Fig. 7e). In the following period (2015–19), mean elevation decreased by 3.03 ± 0.07 m along EE' (Fig. 7f). Telen Glacier showed a similar trend to Skallen Glacier. Along the ICESat-2 track FF' located 0–1 km downglacier from the grounding line, the surface elevation increased in the period 2012–15 and decreased in the period 2015–19 (Figs 7e, f). The changes observed on Telen Glacier were smaller in magnitude than those observed on Shirase and Skallen glaciers.

5. Discussion

5.1. Drivers of the terminus position changes

Our data revealed synchronous frontal variations of the glaciers flowing into Lützow-Holm Bay. In general, the glaciers advanced
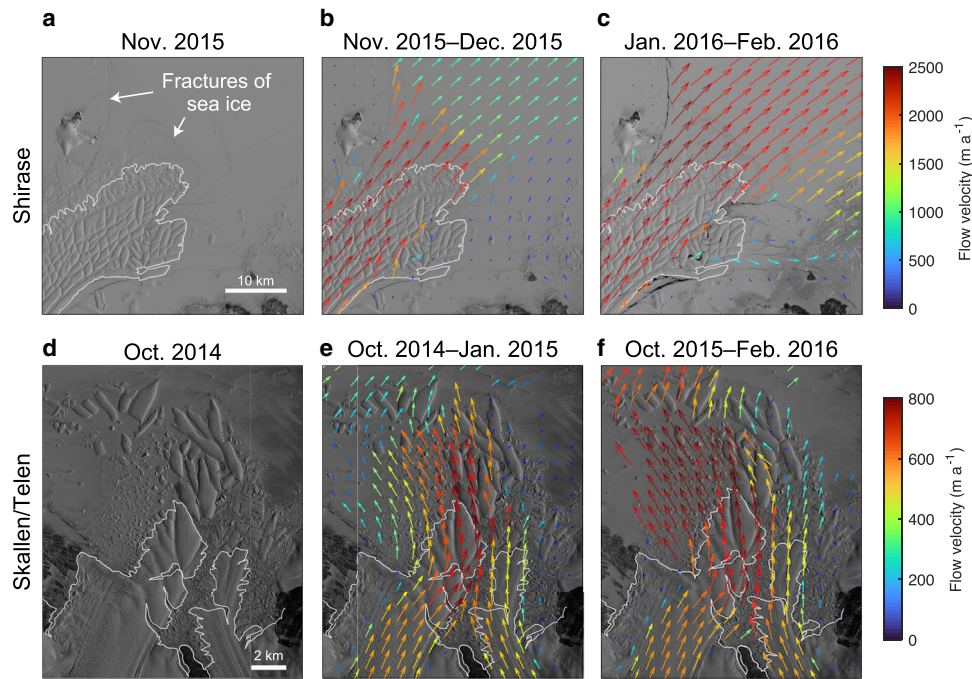
Figure 6. Landsat 8 OLI images showing sea ice and glacier fronts of (a–c) Shirase and (d–f) Skallen/Telen glaciers. The images were acquired on (a and b) 16 November 2015, (c) 3 January 2016, (d and e) 3 October 2014 and (f) 8 October 2015. The color-coded vectors (b, c, e and f) are glacier velocity fields from the indicated periods. The flow vectors are twice as large as the actual distance. The white lines show the glacier margins.

from 1989 to 1997, followed by a period of retreat observed from 1997 to 2000 (Fig. 3). After a period of relatively stable terminus position from 2000 to 2008, the glaciers progressively advanced until a large retreat was initiated in the summers of 2015/16 (Shirase and Langhovde), 2016/17 (Skallen and Honnør) and 2017/18 (Telen) (Fig. 3). The trend observed in this study concurs with previously reported decadal glacier variability in the studied

region, i.e. a retreating trend during the period 1974–90 followed by an advance from 1990 to 2012 (Miles and others, 2016).

The data suggest that the glacier front variations were influenced by sea-ice conditions in Lützow-Holm Bay (Fig. 3). To investigate a possible link between sea ice and the stability of the glacier front, the frontal displacement rate was compared with the SIC anomaly near each glacier front, by taking the
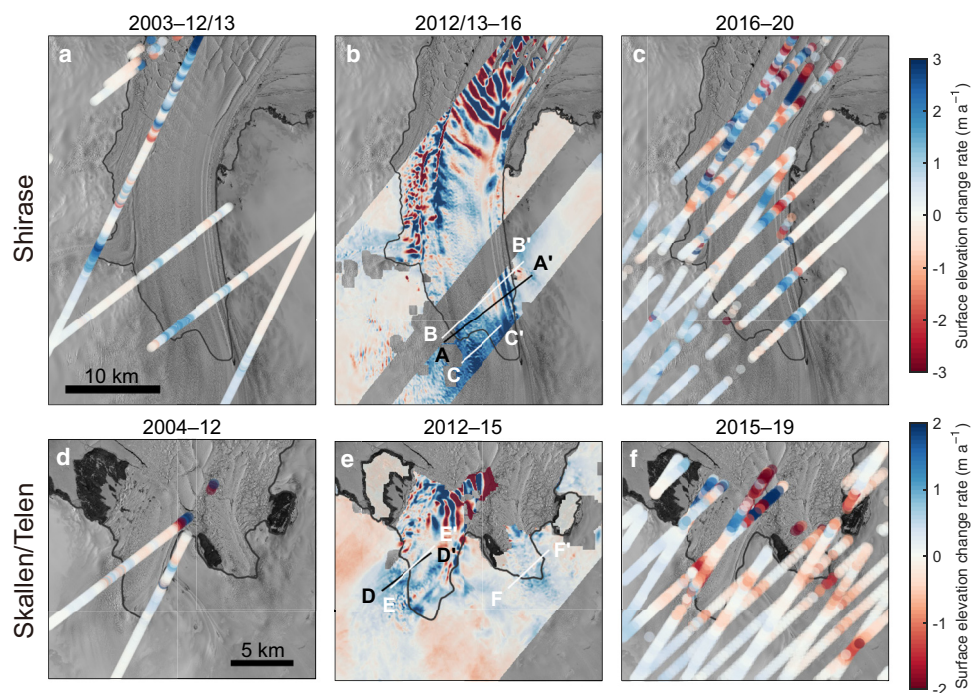

Figure 7. Surface elevation change rates at (a–c) Shirase, (d–f) Skallen/Telen glaciers during the periods (a and d) 2003/04–12/13, (b and e) 2012/13–15/16 and (c and f) 2015/16–19/20. The rates were obtained using elevation data acquired from (a and d) ICESat-1 and REMA, (b and e) REMA and (c and f) REMA and ICESat-2. Elevation changes along the ICESat-1 (AA' and DD') and ICESat-2 tracks (BB', CC', EE', FF') are described in the text and shown in Figure 8. The background is a Landsat 8 OLI image acquired on 3 January 2016.
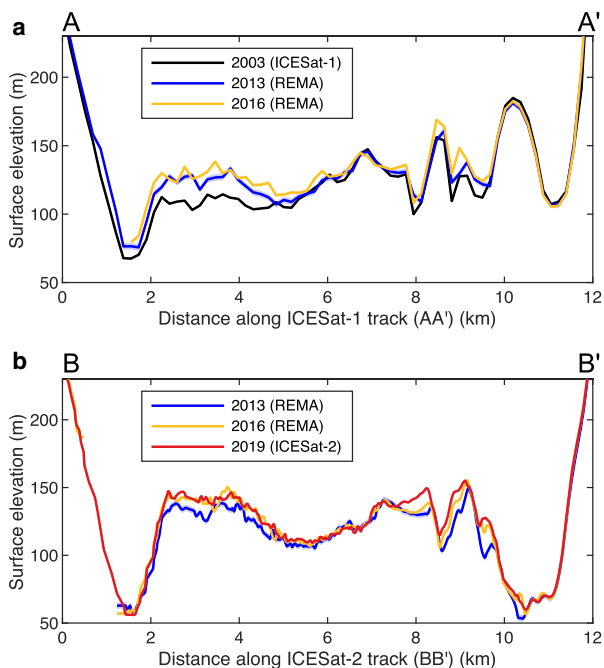
Figure 8. Surface elevation measured near the grounding line of Shirase Glacier along (a) AA' and (b) BB' shown in Figure 7b.

average over every 4-year period from 1992 to 2020. Taking the variability in the flow rates among the glaciers into account, the frontal displacement rates were normalized by the mean ice speed near each glacier terminus. The results illustrate that the glaciers synchronously retreated when the SIC anomaly was substantially negative, whereas they generally advanced during the positive phase (Fig. 9). The displacement rates were dependent on the SIC anomaly with substantially different sensitivities in the positive and negative SIC anomaly ranges ($0.30\%^{-1}$ for negative and $0.01\%^{-1}$ for positive). Excluding the advancing period of 2012–16, there was a significant correlation ($r = 0.77$, $p < 10^{-4}$) between the SIC anomaly and the normalized frontal displacement rate. During the period 2012–16 (SIC anomaly > 3.5%), all the glaciers advanced without significant ice loss by calving (Fig. 3). The normalized displacement rates during this period were within the range of 0.49–1.00 (Fig. 9), meaning that the glaciers advanced at a rate equal to, or half of, the glacier speed. The
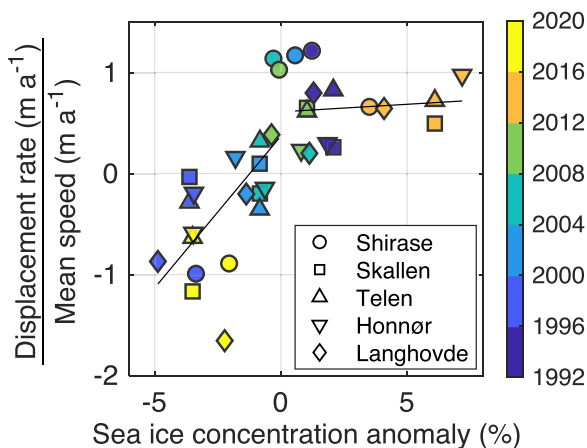
Figure 9. Scatter plot of glacier front displacement rates vs the SIC anomaly near each glacier front. The values for each glacier (symbols) are averaged over every 4-year period (colors). The solid lines show the linear regression of the data in positive and negative SIC anomaly ranges. The displacement rates are normalized by ice speed near the terminus.

most rapid glacier retreat was observed in the period 2016–20, when the SIC anomalies were below −2% after the breakup of land-fast sea ice in 2016 (Fig. 9). Open water was consistently observed near the glacier fronts during the summer months of this period (Figs 3a–e). These observations suggest that stable land-fast sea ice suppressed glacier calving and facilitated the terminus advance in 2008–16. The breakup in 2016 destabilized the glacier termini, resulting in loss of frontal ice. Based on the simultaneous retreat of the glaciers coincident with the sea-ice loss in 1998, 2004 and 2016, we assume that multidecadal glacier front variations on Lützow-Holm Bay are governed by the previously reported periodic breakup of land-fast sea ice occurring at intervals of 10–20 years (Ushio, 2006; Aoki, 2017).

The association of glacier front position with sea-ice condition is in line with previous studies in East Antarctica. Data suggest that tabular iceberg calving is suppressed by the formation of multi-year land-fast sea ice and the development of dense ice mélange in front of the glacier (Massom and others, 2010; Miles and others, 2017; Arthur and others, 2021). A correlation between sea-ice conditions and decadal glacier front variations has been also reported in East Antarctica (Miles and others, 2013, 2016), on the Antarctic Peninsula (Christie and others, 2022) and in the whole of Antarctica (Baumhoer and others, 2021). Our data add to this set of observations that highlight the influence of sea ice on ice-shelf extent with a finer temporal resolution.

5.2. Mechanisms of glacier flow changes

Similar changes in ice speeds were observed at Shirase, Skallen and Telen glaciers, i.e. generally decelerating trends from 2011 to 2015, which were followed by acceleration (Figs 4a–c, 5). Because the onset of the speedup in 2015–16 began slightly before the significant glacier retreat occurred during 2016–20 (Fig. 4), the speedup was unlikely to have been caused by the retreat. For example, Telen Glacier retreated by 2.2 km over the period February–September 2018, lagging 2 years behind the onset of the speedup.

Since the glacier speed changes were greater on the ice shelves than on the grounded ice (Fig. 5), we assume that a change near the front affected the force balance of the glacier. Given that the onset of the flow acceleration coincided with the breakup of land-fast sea ice in 2016, a potential driver of the glacier speedup could be a loss of back-stress exerted by sea ice. As shown in Figures 6b and e, sea-ice displacement prior to the breakup in 2016 was substantially smaller than the forward motion of the glacier terminus. During this period, cracks and fractures were observed on the land-fast sea ice in front of Shirase Glacier (satellite image on 16 November 2015, Fig. 6a). These observations imply that a significantly large stress was exerted on the sea ice by the advancing glacier and that this stress impeded the forward glacier motion. The following summer (2016), sea ice sped up to ~90% of the glacier speed (Fig. 6c), implying that the sea ice lost support from the land and began to move with the glacier front. After the summer of 2015/16, an acceleration of the grounded ice and an even greater speedup of the ice shelves was observed at Shirase, Skallen and Telen glaciers. These observations suggest that the multi-year land-fast sea ice was firmly anchored to the coast and resisted the glacier flow before 2016, whereas the increased mobility of the sea ice resulted in a reduction in resistive stress and subsequent glacier acceleration. Thus, we assume that the land-fast sea ice near the glacier front affected the glacier dynamics.

It is likely that multi-year land-fast sea ice and ice mélange in Lützow-Holm Bay had thickened since 2008 and had become rigid enough to generate stress which added resistance to the glacier flow. During the period of deceleration from 2010 to 2015,

the condition of the sea ice in front of the studied glaciers was probably similar to those reported at Brunt/Stancomb-Wills Ice Shelf and the Larsen B embayment (Khazendar and others, 2009; Rott and others, 2018), where the flow speeds were thought to have been reduced by sea ice/ice mélange accumulated near the glacier fronts.

Ice discharge from Shirase Glacier decreased from 12.7 to 12.5 Gt a^{-1} during the period of deceleration from 2013 to 2015. The change expected from the deceleration was -0.4 Gt a^{-1}, but 33% of the discharge was cancelled by a thickening of the grounded ice during the same period. Our analysis highlights the significant influence of both ice speed and ice thickness on glacier discharge, as well as the impact of sea-ice variations on ice-sheet mass balance.

5.3. Elevation change of the ice sheet

Surface elevation change indicated thickening of Shirase, Skallen and Telen glaciers in 2003/04–15/16 (Figs 7, 8) during the period of glacier deceleration (Fig. 4). The greatest elevation change occurred near the grounding line of Shirase Glacier (2.2 ± 0.1 m a^{-1}) (Figs 7, 8) and was far greater than the surface mass balance reported along the Soya Coast (<0.4 m w.e. a^{-1}) (Motoyama and others, 2008, 2015; Wang and others, 2015). Shirase, Skallen and Telen glaciers began thinning in 2016, in response to the acceleration of the glaciers, suggesting a link between flow regime and ice thickness (e.g. Pritchard and others, 2009). Since the observed ice speed changes were greater on the ice shelves as compared to the grounded ice (Fig. 5), the stretching ice flow along the glacier should have been reduced/enhanced by deceleration/acceleration. According to the strain rate analysis, the longitudinal (parallel to the flow direction) component of the strain rate tensor from the velocity fields in 2018 shows stretching flow regimes near the grounding line of Shirase, Skallen and Telen glaciers (Fig. 10). A positive (stretching) strain rate exceeding 0.1 a^{-1} was observed near the grounding line of the three glaciers. At Shirase Glacier, the greatest strain rate of 0.14 a^{-1} occurred near the western margin (Fig. 10a, near A and B), where the largest surface elevation change was observed in the period 2003–16 (Figs 7, 8).

Further analysis demonstrated the impact of the ice speed change on the strain rate regime. The magnitude of the deceleration from 2007 to 2015 was greater on the ice shelf than on the grounded area (Figs 11a–c), which resulted in a reduction in the stretching flow and an increase in the vertical strain rate near the grounding line and the upper reaches (Figs 11d–f). The increase in the vertical strain rate implies a thickening, consistent with the surface uplift observed near the grounding line at Shirase, Skallen and Telen glaciers (Figs 11g–i). In the following period (2015–18), the vertical strain rate decreased as a result of the speedup, which was more pronounced over the ice shelf (Figs 11a–f). The enhanced stretching flow regime is consistent with the decrease in surface elevation at Shirase, Skallen and Telen glaciers (Figs 11g–i). These results strongly suggest that the increase and decrease in elevation during the periods of deceleration and acceleration was driven by the changes in the vertical strain rate.

Our data also indicated that the observed change in ice thickness affected the grounding line positions. From 2012/13 to 2016, during the period of deceleration and thickening, the grounding line of Shirase Glacier estimated from surface slope showed seaward advance by 65 m (20 m a^{-1}). This observation is consistent with a previous measurement with CryoSat-2 altimetry data, i.e. an advance at a rate of 14.7 m a^{-1} between 2010 and 2016 (Konrad and others, 2018). Skallen and Telen glaciers also showed seaward grounding line migration of 7 and 18 m between 2012
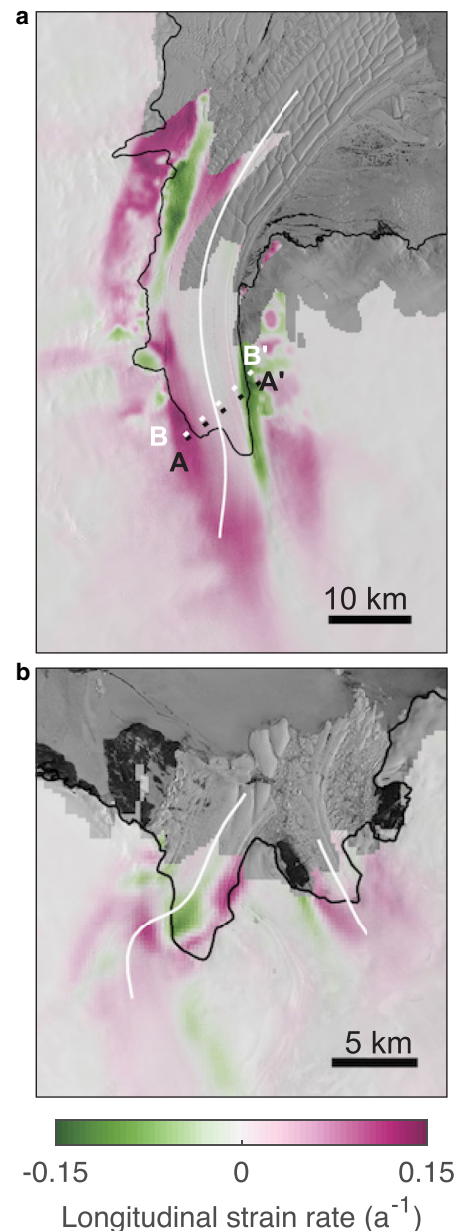

Figure 10. Longitudinal strain rate distributions calculated from the glacier flow velocity in 2018 from the ITS_LIVE dataset at (a) Shirase and (b) Skallen/Telen glaciers. The white lines show the central flowlines used for Figure 11. The background is a Landsat 8 OLI image acquired on 8 January 2018.

and 2015. The changes in grounding line position affect the ice motion near the grounding line because of changes in basal stress (e.g. Payne and others, 2004), thus a complex feedback mechanism is expected between the changes in ice speed and ice thickness triggered by variations in land-fast sea ice.

6. Conclusions

To investigate recent glacier variations in Lützow-Holm Bay, East Antarctica, we measured the front position, flow velocity and surface elevation of five outlet glaciers from 1988 to 2020. The glacier variations observed were compared with sea-ice conditions near the glacier fronts to elucidate a possible link with variations in sea ice.

The glacier fronts simultaneously advanced from 2008 to 2015, at which time the ocean immediately adjacent to the ice fronts was largely covered with sea ice. All the glaciers rapidly retreated in
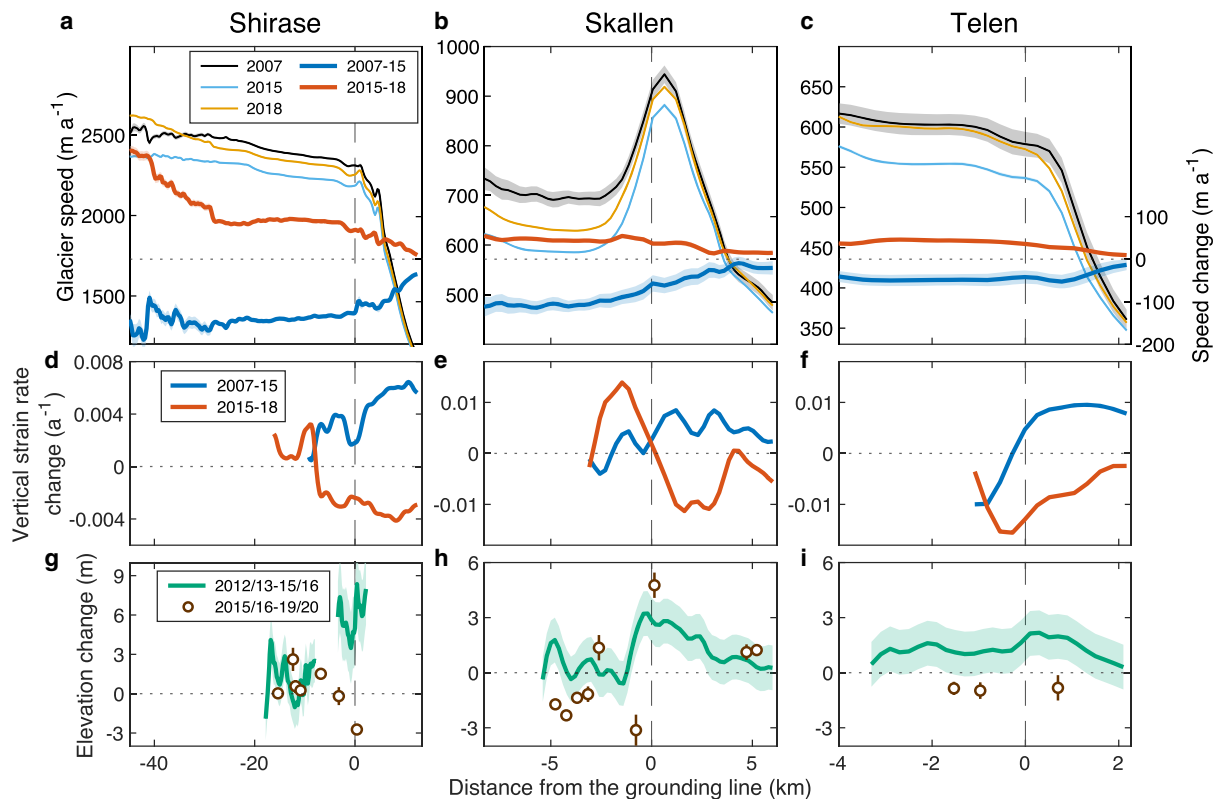
Figure 11. (a–c) Glacier speed in 2007 (black), 2015 (light blue) and 2018 (orange) along the central flowline shown in Figure 10. Speed changes across the periods 2007–2015 (blue) and 2015–2018 (red) are also shown. (d–f) Changes in the vertical strain rate computed from the glacier velocity field. (g–i) Elevation changes in 2012/13–15/16 (green) and 2015/16–19/20 (circles). Vertical dashed lines indicate the location of the grounding line.

the period 2016–18, which coincided with a major breakup of land-fast sea ice in Lützow-Holm Bay in 2016. The breakup was the most significant sea-ice loss since 1998. The retreat rate of the glaciers correlated with the SIC anomaly near the glacier fronts, suggesting that sea ice is a factor which controls terminus variations. Shriase, Skallen and Telen glaciers decelerated in the period 2011–15 and accelerated in 2016–18. These flow speed changes were most pronounced on the ice shelves but were also observed upstream of the grounding line. Sea-ice motion and fractures near the glacier fronts suggested a large stress acting at the interface of the glacier and sea ice during the deceleration period. The glacier flow accelerated when the sea ice became mobile, and its buttressing stress reduced after the breakup in 2016. Glacier thickness was also affected by the sea-ice breakup and the associated ice speed change. Near the grounding lines of Shirase, Skallen and Tellen glaciers, the thickness increased/decreased during the deceleration/acceleration periods, respectively. An analysis of the strain rate suggested that the changes in the glacier flow regime affected the thickness by changing the vertical strain rate.

Our data demonstrate that the presence of land-fast sea ice affects glacier speed and ice thickness, as well as glacier front variations. Therefore, sea-ice variations in front of glaciers may trigger a complex feedback mechanism between glacier flow and ice thickness. Given that sea ice is highly sensitive to climate (Heil, 2006; Fraser and others, 2012; Aoki, 2017), an accurate understanding of land-fast sea ice is crucial for the projection of glacier changes in Antarctica in a changing climate.

Data. Landsat images were downloaded from the US Geological Survey Earth Explorer (http://earthexplorer.usgs.gov/). JERS-1 SAR images were available from JAXA G-Portal (https://gportal.jaxa.jp/gpr/). The REMA DEMs were downloaded via https://www.pgc.umn.edu/data/rema/. The ITS_LIVE, Climate Data Record of Passive Microwave Sea Ice Concentration, Version 4 and BedMachine Antarctica, Version 3 were downloaded from NOAA

NSIDC (https://nsidc.org/). The CryoSat-2 data are available from European Space Agency CryoTEMPO project (https://cryotempo-eolis.org/). The ICESat-1/2 data were downloaded via OpenAltimetry (https://openaltimetry.org/). The dataset of air temperature at Syowa Station is available from the Japanese Meteorological Agency (https://www.jma.go.jp/).

References

Alley KE and 5 others (2018) Continent-wide estimates of Antarctic strain rates from Landsat 8-derived velocity grids. *Journal of Glaciology* **64**(244), 321–332. doi: 10.1017/jog.2018.23

Aoki S (2017) Breakup of land-fast sea ice in Lützow-Holm Bay, East Antarctica, and its teleconnection to tropical Pacific sea surface temperatures. *Geophysical Research Letters* **44**(7), 3219–3227. doi: 10.1002/2017GL072835

Arthur JF and 5 others (2021) The triggers of the disaggregation of Voyeykov Ice Shelf (2007), Wilkes Land, East Antarctica, and its subsequent evolution. *Journal of Glaciology* **67**(265), 933–951. doi: 10.1017/jog.2021.45

Baumhoer CA, Dietz AJ, Kneisel C, Paeth H and Kuenzer C (2021) Environmental drivers of circum-Antarctic glacier and ice shelf front retreat over the last two decades. *The Cryosphere* **15**(5), 2357–2381. doi: 10.5194/tc-15-2357-2021

Bindschadler R and 17 others (2011) Getting around Antarctica: new high-resolution mappings of the grounded and freely-floating boundaries of the Antarctic ice sheet created for the International Polar Year. *The Cryosphere* **5**(3), 569–588. doi: 10.5194/tc-5-569-2011

Brunt KM, Neumann TA and Smith BE (2019) Assessment of ICESat-2 ice sheet surface heights, based on comparisons over the interior of the Antarctic ice sheet. *Geophysical Research Letters* **46**(22), 13072–13078. doi: 10.1029/2019GL084886

Christianson K and 19 others (2016) Sensitivity of Pine Island Glacier to observed ocean forcing: PIG response to ocean forcing. *Geophysical Research Letters* **43**(20), 10817–10825. doi: 10.1002/2016GL070500

Christie FDW and 5 others (2022) Antarctic ice-shelf advance driven by anomalous atmospheric and sea-ice circulation. *Nature Geoscience* **15**, 356–362. doi: 10.1038/s41561-022-00938-x

Dupont TK and Alley RB (2005) Assessment of the importance of ice-shelf buttressing to ice-sheet flow. *Geophysical Research Letters* **32**(4), L04503. doi: 10.1029/2004GL022024

Dutrieux P and 9 others (2014) Strong sensitivity of Pine Island ice-shelf melting to climatic variability. *Science* **343**(6167), 174–178. doi: 10.1126/science.1244341

Enomoto H, Nishio F, Warashina H and Ushio S (2002) Satellite observation of melting and break-up of fast ice in Lutzow-Holm Bay, East Antarctica. *Polar Meteorology and Glaciology* **16**, 1–14. doi: 10.15094/00002942

Fraser AD, Massom RA, Michael KJ, Galton-Fenzi BK and Lieser JL (2012) East Antarctic Landfast sea ice distribution and variability, 2000–08. *Journal of Climate* **25**(4), 1137–1156. doi: 10.1175/JCLI-D-10-05032.1

Fricker HA and Padman L (2006) Ice shelf grounding zone structure from ICESat laser altimetry. *Geophysical Research Letters* **33**(15), L15502. doi: 10.1029/2006GL026907

Fukuda T (2014) Variations in the terminus position, ice velocity and surface elevation of the Langhovde Glacier, East Antarctica (PhD Thesis). Hokkaido University. doi: 10.14943/doctoral.k11345

Fukuda T, Sugiyama S, Sawagaki T and Nakamura K (2014) Recent variations in the terminus position, ice velocity and surface elevation of Langhovde Glacier, East Antarctica. *Antarctic Science* **26**(6), 636–645. doi: 10.1017/S0954102014000364

Fürst JJ and 6 others (2016) The safety band of Antarctic ice shelves. *Nature Climate Change* **6**(5), 479–482. doi: 10.1038/nclimate2912

Gardner AS and 6 others (2018) Increased West Antarctic and unchanged East Antarctic ice discharge over the last 7 years. *The Cryosphere* **12**(2), 521–547. doi: 10.5194/tc-12-521-2018

Gardner AS, Fahnestock MA and Scambos TA (2019) ITS_LIVE regional glacier and ice sheet surface velocities: Version 1. *Data archived at National Snow and Ice Data Center*. doi: 10.5067/6II6VW8LLWJ7

Gourmelen N and 8 others (2018) CryoSat-2 swath interferometric altimetry for mapping ice elevation and elevation change. *Advances in Space Research* **62**(6), 1226–1242. doi: 10.1016/j.asr.2017.11.014

Hall DK, Riggs GA and Salomonson VV (1995) Development of methods for mapping global snow cover using moderate resolution imaging spectroradiometer data. *Remote Sensing of Environment* **54**(2), 127–140. doi: 10.1016/0034-4257(95)00137-P

Heid T and Kääb A (2012) Evaluation of existing image matching methods for deriving glacier surface displacements globally from optical satellite imagery. *Remote Sensing of Environment* **118**, 339–355. doi: 10.1016/j.rse.2011.11.024

Heil P (2006) Atmospheric conditions and fast ice at Davis, East Antarctica: a case study. *Journal of Geophysical Research* **111**(C5), C05009. doi: 10.1029/2005JC002904

Hirano D and 10 others (2020) Strong ice-ocean interaction beneath Shirase Glacier Tongue in East Antarctica. *Nature Communications* **11**, 4221. doi: 10.1038/s41467-020-17527-4

Howat IM, Box JE, Ahn Y, Herrington A and McFadden EM (2010) Seasonal variability in the dynamics of marine-terminating outlet glaciers in Greenland. *Journal of Glaciology* **56**(198), 601–613. doi: 10.3189/002214310793146232

Howat IM, Porter C, Smith BE, Noh M and Morin P (2019) The reference elevation model of Antarctica. *The Cryosphere* **13**, 665–674. doi: 10.5194/tc-13-665-2019

The IMBIE team (2018) Mass balance of the Antarctic Ice Sheet from 1992 to 2017. *Nature* **558**, 219–222. doi: 10.1038/s41586-018-0179-y

Jacobs SS, Jenkins A, Giulivi CF and Dutrieux P (2011) Stronger ocean circulation and increased melting under Pine Island Glacier ice shelf. *Nature Geoscience* **4**, 519–523. doi: 10.1038/ngeo1188

Khalsa SJS and 8 others (2020) OpenAltimetry – rapid analysis and visualization of Spaceborne altimeter data. *Earth Science Informatics* **15**, 1471–1480. doi: 10.1007/s12145-020-00520-2

Khazendar A, Rignot E and Larour E (2009) Roles of marine ice, rheology, and fracture in the flow and stability of the Brunt/Stancomb-Wills Ice Shelf. *Journal of Geophysical Research: Earth Surface* **114**(F4), F04007. doi: 10.1029/2008JF001124

Konrad H and 6 others (2018) Net retreat of Antarctic glacier grounding lines. *Nature Geoscience* **11**, 258–262. doi: 10.1038/s41561-018-0082-z

Kusahara K, Hirano D, Fujii M, Fraser AD and Tamura T (2021) Modeling intensive ocean–cryosphere interactions in Lützow-Holm Bay, East Antarctica. *The Cryosphere* **15**, 1697–1717. doi: 10.5194/tc-15-1697-2021

Lea JM (2018) The Google Earth Engine Digitisation Tool (GEEDiT) and the Margin change Quantification Tool (MaQiT) – simple tools for the rapid mapping and quantification of changing Earth surface margins. *Earth Surface Dynamics* **6**(3), 551–561. doi: 10.5194/esurf-6-551-2018

Lea JM, Mair DWF and Rea BR (2014) Evaluation of existing and new methods of tracking glacier terminus change. *Journal of Glaciology* **60**(220), 323–332. doi: 10.3189/2014JoG13J061

Levinsen JF, Howat IM and Tscherning CC (2013) Improving maps of ice-sheet surface elevation change using combined laser altimeter and stereoscopic elevation model data. *Journal of Glaciology* **59**(215), 524–532. doi: 10.3189/2013JoG12J114

Mae S and Naruse R (1978) Possible causes of ice sheet thinning in the Mizuho Plateau. *Nature* **273**, 291–292. doi: 10.1038/273291a0

Mae S and Yoshida M (1987) Airborne radio echo sounding in Shirase Glacier drainage basin, Antarctica. *Annals of Glaciology* **9**, 160–165. doi: 10.3189/S0260305500000549

Massom RA and 7 others (2010) Examining the interaction between multi-year landfast sea ice and the Mertz Glacier Tongue, East Antarctica: another factor in ice sheet stability? *Journal of Geophysical Research: Oceans* **115**(C12), C12027. doi: 10.1029/2009JC006083

Massom RA and 5 others (2018) Antarctic ice shelf disintegration triggered by sea ice loss and ocean swell. *Nature* **558**, 383–389. doi: 10.1038/s41586-018-0212-1

Meier WN, Fetterer F, Windnagel AK and Stewart JS (2021) *NOAA/NSIDC Climate Data Record of Passive Microwave Sea Ice Concentration, Version 4*. Boulder, Colorado, USA: NSIDC: National Snow and Ice Data Center. doi: 10.7265/efmz-2t65

Miles BWJ and 5 others (2023) Slowdown of Shirase Glacier, East Antarctica, caused by strengthening alongshore winds. *The Cryosphere* **17**(1), 445–456. doi: 10.5194/tc-17-445-2023

Miles BWJ, Stokes CR and Jamieson SSR (2016) Pan–ice-sheet glacier terminus change in East Antarctica reveals sensitivity of Wilkes Land to sea-ice changes. *Science Advances* **2**(5), e1501350. doi: 10.1126/sciadv.1501350

Miles BWJ, Stokes CR and Jamieson SSR (2017) Simultaneous disintegration of outlet glaciers in Porpoise Bay (Wilkes Land), East Antarctica, driven by sea ice break-up. *The Cryosphere* **11**(1), 427–442. doi: 10.5194/tc-11-427-2017

Miles BWJ, Stokes CR, Vieli A and Cox NJ (2013) Rapid, climate-driven changes in outlet glaciers on the Pacific coast of East Antarctica. *Nature* **500**, 563–566. doi: 10.1038/nature12382

Minowa M, Podolskiy EA and Sugiyama S (2019) Tide-modulated ice motion and seismicity of a floating glacier tongue in East Antarctica. *Annals of Glaciology* **60**(79), 57–67. doi: 10.1017/aog.2019.25

Morlighem M and 36 others (2020) Deep glacial troughs and stabilizing ridges unveiled beneath the margins of the Antarctic ice sheet. *Nature Geoscience* **13**, 132–137. doi: 10.1038/s41561-019-0510-8

Morlighem M (2022) *MEaSUREs BedMachine Antarctica, Version 3*. Boulder, Colorado, USA: NSIDC: National Snow and Ice Data Center. doi: doi.org/10.5067/FPSU0V1MWUB6

Motoyama H and 7 others (2008) Glaciological data collected by the 45th, 46th and 47th Japanese Antarctic research expeditions during 2004–2007. *JARE Data Reports. Glaciology* **34**, 1–22. doi: 10.15094/00005005

Motoyama and 25 others (2015) Glaciological data collected by the 48th–54th Japanese Antarctic research expeditions during 2007–2013. *JARE Data Reports. Glaciology* **35**, 1–44. doi: 10.15094/00010905

Mouginot J, Rignot E and Scheuchl B (2014) Sustained increase in ice discharge from the Amundsen Sea Embayment, West Antarctica, from 1973 to 2013. *Geophysical Research Letters* **41**(5), 1576–1584. doi: 10.1002/2013GL059069

Moussavi M and 5 others (2020) Antarctic supraglacial lake detection using Landsat 8 and Sentinel-2 imagery: towards continental generation of lake volumes. *Remote Sensing* **12**(1), 134. doi: 10.3390/RS12010134

Nakamura K, Aoki S, Yamanokuchi T and Tamura T (2022) Interactive movements of outlet glacier tongue and Landfast sea ice in Lützow-Holm

Bay, East Antarctica, detected by ALOS-2/PALSAR-2 imagery. *Science of Remote Sensing* **6**, 100064. doi: 10.1016/j.srs.2022.100064

Nakamura K, Doi K and Shibuya K (2010) Fluctuations in the flow velocity of the Antarctic Shirase Glacier over an 11-year period. *Polar Science* **4**(3), 443–455. doi: 10.1016/j.polar.2010.04.010

Naruse R (1979) Thinning of the ice sheet in Mizuho Plateau, East Antarctica. *Journal of Glaciology* **24**(90), 45–52. doi: 10.1017/S0022143000014635

Nick F, Vieli A, Howat I and Joughin I (2009) Large-scale changes in Greenland outlet glacier dynamics triggered at the terminus. *Nature Geoscience* **2**, 110–114. doi: 10.1038/ngeo394

Nuth C and Kääb A (2011) Co-registration and bias corrections of satellite elevation data sets for quantifying glacier thickness change. *The Cryosphere* **5**(1), 271–290. doi: 10.5194/tc-5-271-2011

Nye JF (1959) A method of determining the strain-rate tensor at the surface of a glacier. *Journal of Glaciology* **3**(25), 409–419. doi: 10.3189/s0022143000017093

Pattyn F and Derauw D (2002) Ice-dynamic conditions of Shirase Glacier, Antarctica, inferred from ERS SAR interferometry. *Journal of Glaciology* **48**(163), 559–565. doi: 10.3189/172756502781831115

Payne AJ, Vieli A, Shepherd AP, Wingham DJ and Rignot E (2004) Recent dramatic thinning of largest West Antarctic ice stream triggered by oceans. *Geophysical Research Letters* **31**(23), L23401. doi: 10.1029/2004GL021284

Pritchard HD, Arthern RJ, Vaughan DG and Edwards LA (2009) Extensive dynamic thinning on the margins of the Greenland and Antarctic ice sheets. *Nature* **461**, 971–975. doi: 10.1038/nature08471

Rignot E (2004) Accelerated ice discharge from the Antarctic Peninsula following the collapse of Larsen B ice shelf. *Geophysical Research Letters* **31**(18), L18401. doi: 10.1029/2004GL020697

Rignot E and 5 others (2019) Four decades of Antarctic ice sheet mass balance from 1979–2017. *Proceedings of the National Academy of Sciences* **116**(4), 1095–1103. doi: 10.1073/pnas.1812883116

Rignot E, Mouginot J, Morlighem M, Seroussi H and Scheuchl B (2014) Widespread, rapid grounding line retreat of Pine Island, Thwaites, Smith, and Kohler glaciers, West Antarctica, from 1992 to 2011. *Geophysical Research Letters* **41**(10), 3502–3509. doi: 10.1002/2014GL060140

Rott H and 8 others (2018) Changing pattern of ice flow and mass balance for glaciers discharging into the Larsen A and B embayments, Antarctic Peninsula, 2011 to 2016. *The Cryosphere* **12**(4), 1273–1291. doi: 10.5194/tc-12-1273-2018

Sakakibara D and Sugiyama S (2014) Ice-front variations and speed changes of calving glaciers in the Southern Patagonia Icefield from 1984 to 2011. *Journal of Geophysical Research* **119**(11), 2541–2554. doi: 10.1002/2014JF003148

Sakakibara D and Sugiyama S (2020) Seasonal ice-speed variations in 10 marine-terminating outlet glaciers along the coast of Prudhoe Land, northwestern Greenland. *Journal of Glaciology* **66**(255), 25–34. doi: 10.1017/jog.2019.81

Shepherd A and 9 others (2019) Trends in Antarctic Ice Sheet elevation and mass. *Geophysical Research Letters* **46**(14), 8174–8183. doi: 10.1029/2019GL082182

Shepherd A, Wingham D and Rignot E (2004) Warm ocean is eroding West Antarctic Ice Sheet. *Geophysical Research Letters* **31**(23), L23402. doi: 10.1029/2004GL021106

Shiramizu K (2018) A study on the estimation of spatio-temporal flow distribution in the Antarctic ice sheet using synthetic aperture radar data (PhD thesis). Sokendai University, (in Japanese).

Shuman CA and 6 others (2006) ICESat Antarctic elevation data: preliminary precision and accuracy assessment. *Geophysical Research Letters* **33**(7), L07501. doi: 10.1029/2005GL025227

Smith B and 14 others (2020a) Pervasive ice sheet mass loss reflects competing ocean and atmosphere processes. *Science* **368**(6496), 1239–1242. doi: 10.1126/science.aaz5845

Smith B and 9 others (2020b) *ATLAS/ICESat-2 L3A Land Ice Height, Version 3*. Boulder, Colorado, USA: NASA National Snow and Ice Data Center Distributed Active Archive Center. doi: 10.5067/ATLAS/ATL06.003

Sugiyama S, Sawagaki T, Fukuda T and Aoki S (2014) Active water exchange and life near the grounding line of an Antarctic outlet glacier. *Earth and Planetary Science Letters* **399**, 52–60. doi: 10.1016/j.epsl.2014.05.001

Ushio S (2006) Factors affecting fast-ice break-up frequency in Lützow-Holm Bay, Antarctica. *Annals of Glaciology* **44**, 177–182. doi: 10.3189/172756406781811835

Ushio S, Wakabayashi H and Nishio F (2006) Sea ice variation in Lützow-Holmbukta, Antarctica, during the last fifty years. *Seppyo* **68**(4), 299–305, (in Japanese).

Wada M and Mae S (1981) Airborne radio echo sounding on the Shirase glacier and its drainage basin, East Antarctica. *Antarctic Record* **72**, 16–25. doi: 10.15094/00008239

Wang Y and 5 others (2015) Recent surface mass balance from Syowa Station to Dome F, East Antarctica: comparison of field observations, atmospheric reanalyses, and a regional atmospheric climate model. *Climate Dynamics* **45**, 2885–2899. doi: 10.1007/s00382-015-2512-6

Wuite J and 7 others (2015) Evolution of surface velocities and ice discharge of Larsen B outlet glaciers from 1995 to 2013. *The Cryosphere* **9**(3), 957–969. doi: 10.5194/tc-9-957-2015

Zwally HJ and 7 others (2014) *GLAS/ICESat L1B Global Elevation Data, Version 34*. Boulder, Colorado, USA. NASA National Snow and Ice Data Center Distributed Active Archive Center. doi: 10.5067/ICESAT/GLAS/DATA126